Vicinal Co Atoms Coordinated Fe-N-C Catalysts to Boost the Oxygen Reduction Reaction

Yubin Chen[a,b], Jiejie Li[c], Yanping Zhu[a,b], Jian Zou[a,b], Hao Zhao[a,b], Chi Chen[*a], Qingqing Cheng[a], Bo Yang[c], Liangliang Zou[a] Zhiqing Zou[a], Hui Yang[*a]

a. Shanghai Advanced Research Institute, Chinese Academy of Sciences, Shanghai 201210, China;

b. University of Chinese Academy of Sciences, Beijing 100049, China

c. School of Physical Science and Technology, ShanghaiTech University, Shanghai, 201210, China.

** Corresponding author, E-mail: chenchi@sari.ac.cn; chengqq@sari.ac.cn and yangh@sari.ac.cn*

Experimental Section

Synthesis of FeCo-ZIF8-X

Typically, 3.284 g 2-methylimidazole was dissolved in 500 mL methanol with stirring. Then 500 mL methanol containing 2.975 g $Zn(NO_3)_2 \cdot 6H_2O$, 244 mg $Fe(NO_3)_3 \cdot 9H_2O$ and a certain amount of $Co(NO_3)_2 \cdot 6H_2O$ were added with vigorous stirring for 24h at room temperature. The obtained product was separated by centrifugation and washed with ethanol and finally dried at 60℃ under vacuum for overnight.

Synthesis of Fe-ZIF8

Typically, 3.284 g 2-methylimidazole was dissolved in 500 mL methanol with stirring. Then 500 mL methanol containing 2.975 g $Zn(NO_3)_2 \cdot 6H_2O$, and 244 mg $Fe(NO_3)_3 \cdot 9H_2O$ were added with vigorous stirring for 24h at room temperature. The obtained product was separated by centrifugation and washed with ethanol and finally dried at 60℃ under vacuum for overnight.

Synthesis of Co-ZIF8

Typically, 3.284 g 2-methylimidazole was dissolved in 500 mL methanol with stirring. Then 500 mL methanol containing 2.975 g $Zn(NO_3)_2 \cdot 6H_2O$, and 660 mg $Co(NO_3)_2 \cdot 6H_2O$ were added with vigorous stirring for 24h at room temperature. The

obtained product was separated by centrifugation and washed with ethanol and finally dried at 60℃ under vacuum for overnight.

Synthesis of FeCo-NC-X

The powder of FeCo-Zn-ZIF-X was placed in a tube furnace and then heated to the 600 ºC for 1 h, and the to the 900 ºC (5 ºC·min^{-1}) for 1 h under flowing Ar atmosphere and finally naturally cooled to room temperature, respectively. The X (X = 1, 2, 3) represents the amount of $Co(NO_3)_2 \cdot 6H_2O$ (220, 440 and 660 mg) used in the synthesis process.

Synthesis of Fe-NC

The powder of Fe-Zn-ZIF was placed in a tube furnace and then heated to the 600 ºC for 1 h, and the to the 900 ºC (5 ºC·min^{-1}) for 1 h under flowing Ar atmosphere and finally naturally cooled to room temperature, respectively.

Synthesis of Co-NC

The powder of Co-Zn-ZIF was placed in a tube furnace and then heated to the 600 ºC for 1 h, and the to the 900 ºC (5 ºC·min^{-1}) for 1 h under flowing Ar atmosphere and finally naturally cooled to room temperature, respectively.

Physical Characterizations

The morphology and crystal of materials were characterized by scanning electron microscopy (SEM, Hitachi Situation-4800), transmission electron microscopy (TEM, FEI Tencnai 30F, 200 kV), high angle annular dark field scanning transmission electron microscopy (HADDF-STEM, FEI Titan Themis G2 60-300) and X-ray diffraction (XRD, Bruker AXS D8 ADVANCE). The content and chemical states of elements were determined by inductively coupled plasma optical emission spectroscopy (ICP-OES, Varian 710-ES) and X-ray photoelectron spectroscopy (XPS, Thermo Fisher Escalab 250 Xi). The surface areas and porosities were determined by measuring the N_2 adsorption-desorption isotherms on Micromeritics ASAP-2020 instrument. The Mössbauer measurements were performed at room temperature (or xx K) using a conventional spectrometer (Germany, Wissel MS-500) in transmission geometry with constant acceleration mode. A ^{57}Co(Rh) source with activity of 25 mCi was used. The velocity calibration was done with a room temperature α-Fe absorber. The spectra were

fitted by the software Recoil using Lorentzian Multiplet Analysis.

Electrochemical Measurements

All electrochemical curves were measured on a CHI 730e electrochemical workstation (CH Instruments) using three-electrode system equipped with a modulated speed rotator (Pine Instruments). To prepare a homogeneous ink containing the catalyst, 6 mg of the catalyst was dispersed in 1 mL of solution containing 950 μL of ethanol and 50 μL of 5% Nafion solution under sonication. While, commercial 20 wt.% Pt/C sample was prepared by dispersing 1 mg of the catalyst in 1 mL of 0.05% Nafion solution. The absolute mass of the catalyst loading was 0.6 mg cm^{-2} for M-N-C and 0.02 mg_{Pt} cm^{-2} for Pt/C. The glassy carbon rotating desk electrode (RDE, diameter is 5 mm, area is 0.196 cm^2) or rotating ring disk electrode (RRDE, diameter is 5.61 mm, area is 0.2475 cm^2) coated with as-prepared catalyst, graphite rod and Hg/Hg_2SO_4 were served as working electrode, counter electrode and reference electrode. All potentials are provided vs RHE.

All the linear sweep voltammetry (LSV) tests with the potential range from 0.1 to 1.1 V vs. RHE were conducted in 0.1 M $HClO_4$ electrolyte with a rotation speed of 900 rpm at a scan rate of 10 mV s^{-1}. RRDE measurements were conducted by LSV at 900 rpm with a scan rate of 10 mV s-1, while the ring electrode was held at 1.2 V vs. RHE. The number of electron transfer (n) and the percent of H_2O_2 were calculated by the following equations:

$$H_2O_2\% = 200 \times \frac{\frac{Ir}{N}}{Id + \frac{Ir}{N}}$$

$$n = 4 \times \frac{Id}{Id + \frac{Ir}{N}}$$

Where I_d is the disk current and I_r is the ring current, N=0.37 (calibrated) is the current collection efficiency of the Pt ring. The ring potential is fixed at 1.3 V vs. RHE.

The Koutecky-Levich (K-L) plots were recorded by RDE measurement at various

rotating speeds from 400 to 2500 rpm. The K-L equation is displayed as followed:

$$\frac{1}{j} = \frac{1}{j_L} + \frac{1}{j_K} = \frac{1}{B\omega^{1/2}} + \frac{1}{j_K}$$

$$B=0.62nFC_0D^{2/3}V^{-1/6}$$

Where J is the measured current density, J_K and J_L are the kinetic and limiting current densities, ω is the angular velocity of the disk, n is the electron transfer number, F is the Faraday constant (96485 C mol^{-1}), C_0 is the bulk concentration of O_2 (1.2×10^{-6} mol cm^{-3}), D_0 is the diffusion coefficient of O_2 in electrolytes (1.9×10^{-5} cm^2 s^{-1}), and V is the kinematic viscosity of the 0.1 M $HClO_4$ (0.0089 cm^2 s^{-1}).

Accelerated durability test (ADT) was conducted by cycling the catalyst with the potentials range from 0.6 to 1.1 V at a scan rate of 50 mV s-1 under continuous purging O_2 in electrolyte.

Proton exchange membrane fuel cell (PEMFC) tests.

For the PEMFCs, Gore (15 um) was selected as the proton exchange membrane. The MEAs with a 2.5 × 2.5 cm^2 active area were fabricated by catalyst coated membrane (CCM) method. The catalyst inks were prepared by dispersing 40% Pt/C (anode) and FeCo-NC (cathode) with 25 wt.% Nafion in isopropanol/H_2O solution under ultrasonic for 3 h. The anode consisted of Pt/C with a metal loading of 0.1 mg cm^{-2}. The cathode consisted of FeCo-NC catalysts with the loading of 3 mg cm^{-2}. The performance of PEMFCs were measured by polarization test on Arbin Fuel Cell Testing System (Arbin Instrument Inc., USA) and the polarization data was recorded per 2 min. The as-prepared MEAs were activated and tested in a PEMFC testing setup by purging H_2 into the anode with the flow rate of 1 standard liter per minute (slpm) and O_2 into the cathode with flow rate of 1 slpm. The testing temperature was controlled at 80 °C with 100 RH% and the back-pressure was fixed at 30 PSIG.

Computational Details

All the spin polarized density functional theory (DFT) calculations were performed within the Vienna Ab-initio Simulation Package (VASP) code.[1, 2] The projected augmented wave (PAW) method was used to model the electron-ion interactions.[3, 4] Generalized gradient approximation (GGA) of BEEF-vdW functional[5] was chosen to

calculate the exchange and correlation energies with explicit long-range dispersion force considered.[6-8] The single FeN_4 and $FeCoN_6$ model were constructed based on a 5×5 slab of graphene (001), as shown in Fig. S16. All the atoms were relaxed during structural optimization. The vacuum height was higher than 15 Å to prevent the interaction between periodic structures. A 2×2×1 k-point grid generated with the Monkhorst-Pack scheme was used.[2] The energy cutoff was set as 500 eV and the convergence criteria was 0.05 eV/Å. A correction with +0.09 eV was used for gas-phase H_2 energies.[9] The free energy of O_2 was obtained with H_2O and H_2 as reference, owing to the poor description of DFT for high-spin ground state of O_2.[10] Solvation stabilization effect was explicitly considered by -0.5 eV for the energy of OH*, -0.35 for OOH*.[1] The computational hydrogen electrode (CHE) model was used for ORR free energy profile calculation.[10] Heat capacities and entropies at 298.15K were referred from previous work.[11]

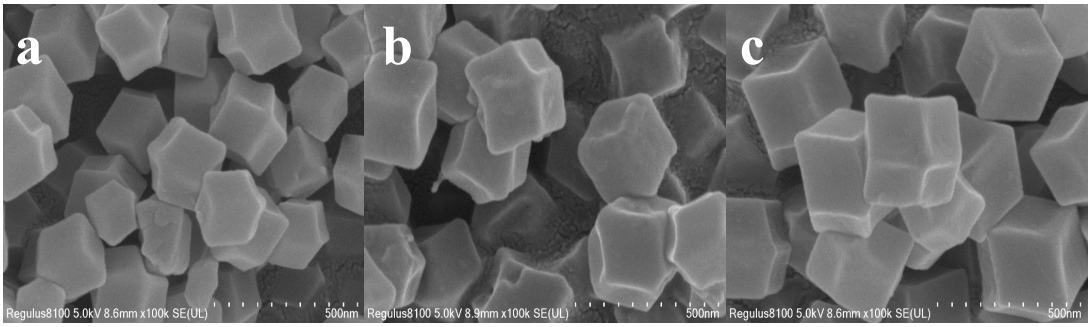

Figure. S1 The SEM images of (a) Fe-ZIF8, (b) FeCo-ZIF8-1 and (c) FeCo-ZIF8-2

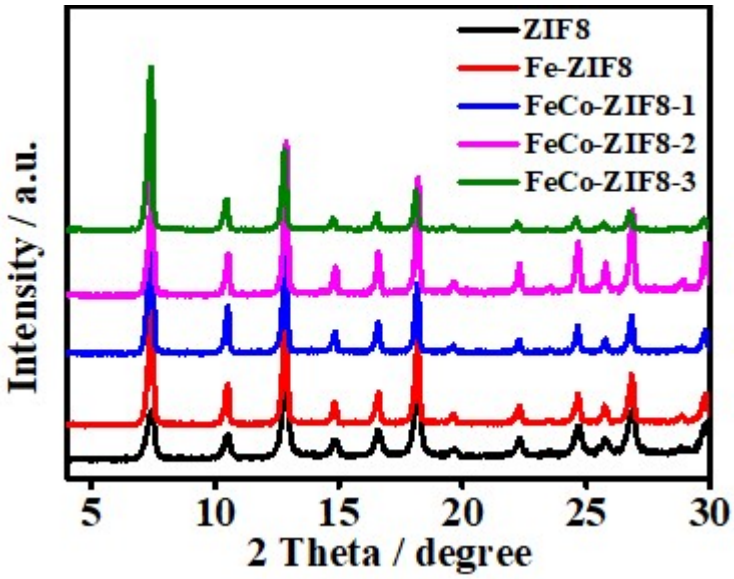

Figure. S2 The XRD patterns of ZIF8, Fe-ZIF8 and FeCo-ZIF8-X

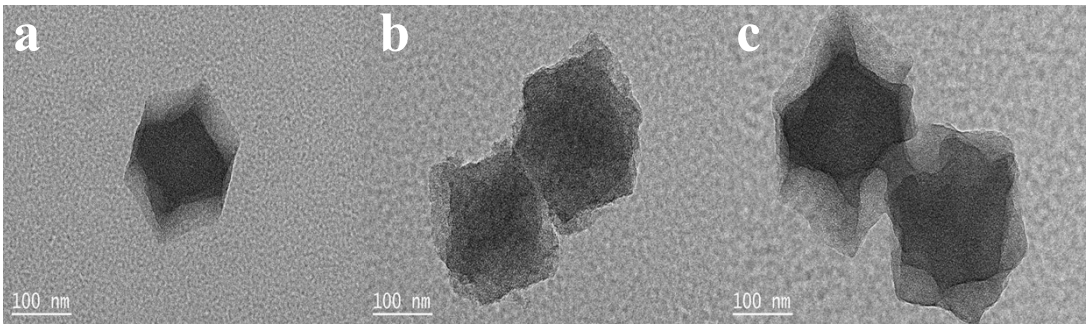

Figure. S3 The TEM images of (a) Fe-NC, (b) FeCo-NC-1 and (c) FeCo-NC-2

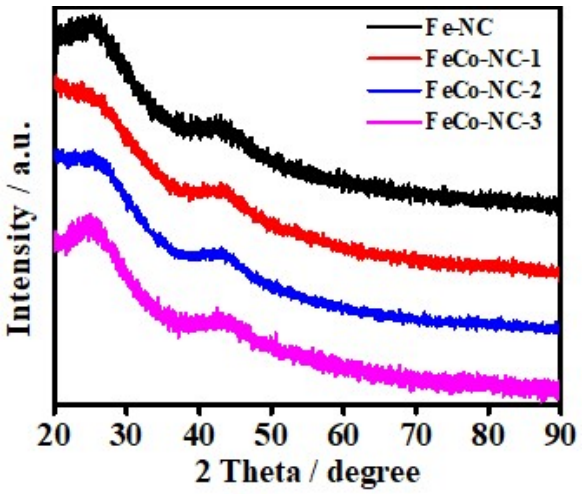

Figure. S4 The XRD patterns of Fe-NC and FeCo-NC-X

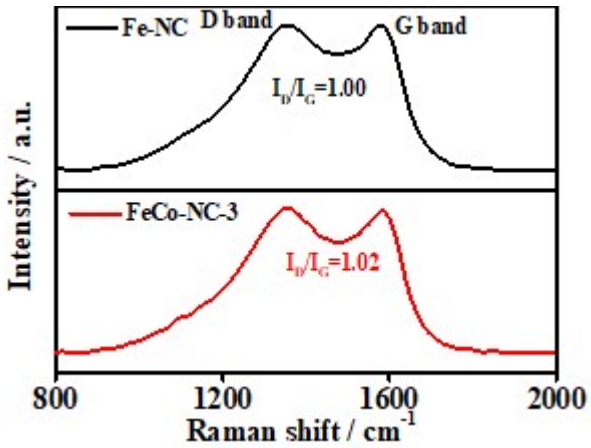

Figure. S5 Raman spectra of Fe-NC and FeCo-NC-3. The intensity ratio of the D band (~1345 cm-1) to G band (~1580 cm-1) (ID/IG) for Fe-NC and FeCo-NC-3 in Raman spectra.

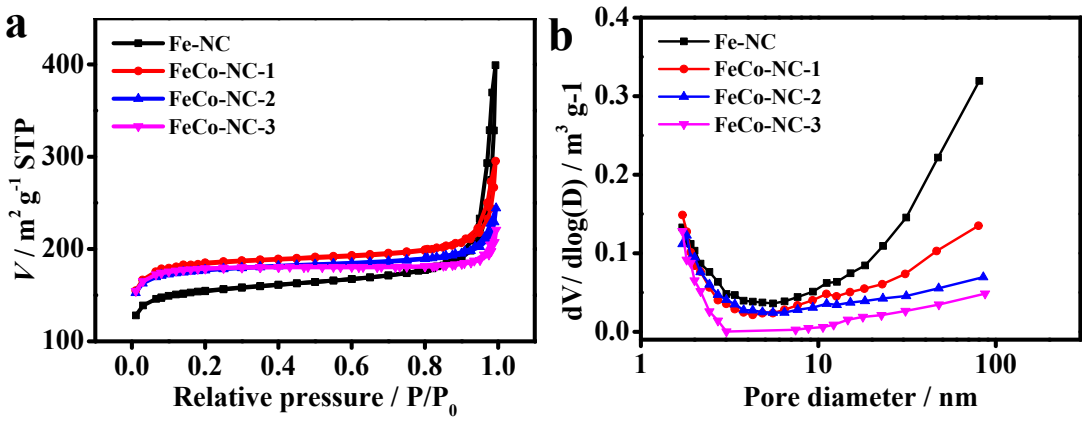

Figure. S6 The N_2 adsorption-desorption isotherms and inset pore size distributions for Fe-NC and FeCo-NC-X

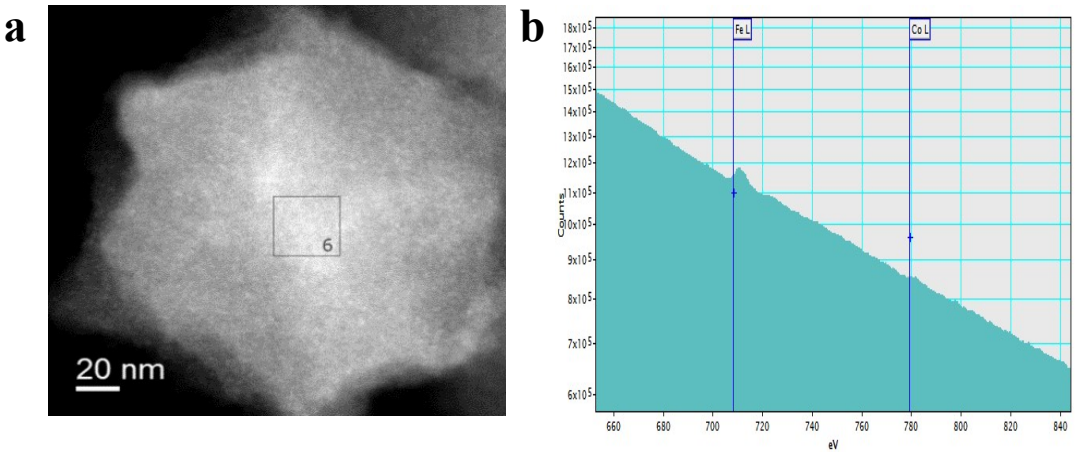

Figure. S7 (a) the selection small area (30 nm× 30 nm) in FeCo-NC-3 and (b) the corresponding EELS spectrum.

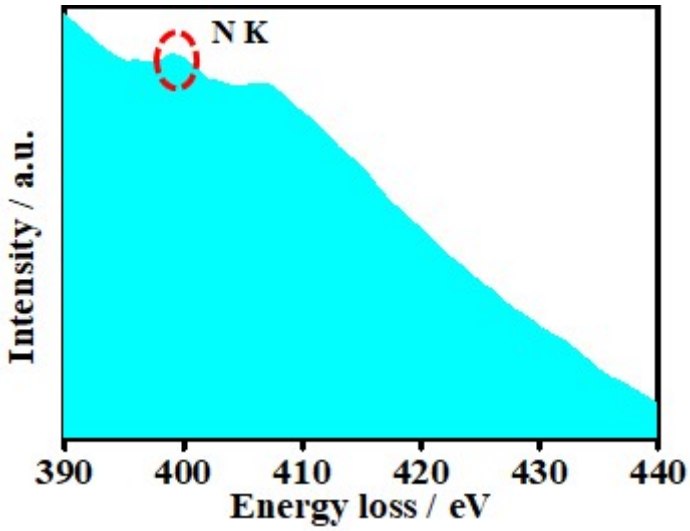

Figure. S8 EELS spectrum of N element for FeCo-NC-3.

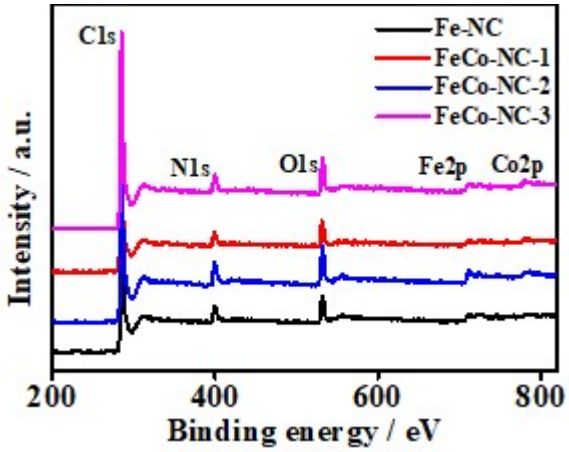

Figure. S9 The XPS survey spectra of Fe-NC and FeCo-NC-X

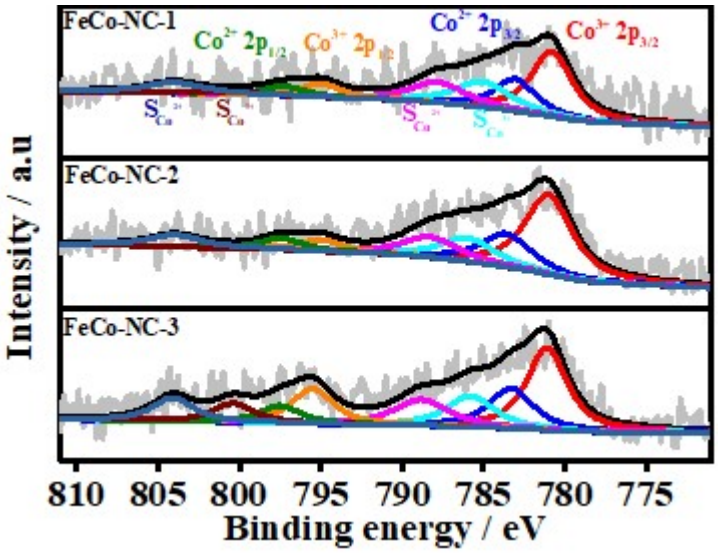

Figure. S10 The high-resolution Co2p XPS spectra of FeCo-NC-X catalysts

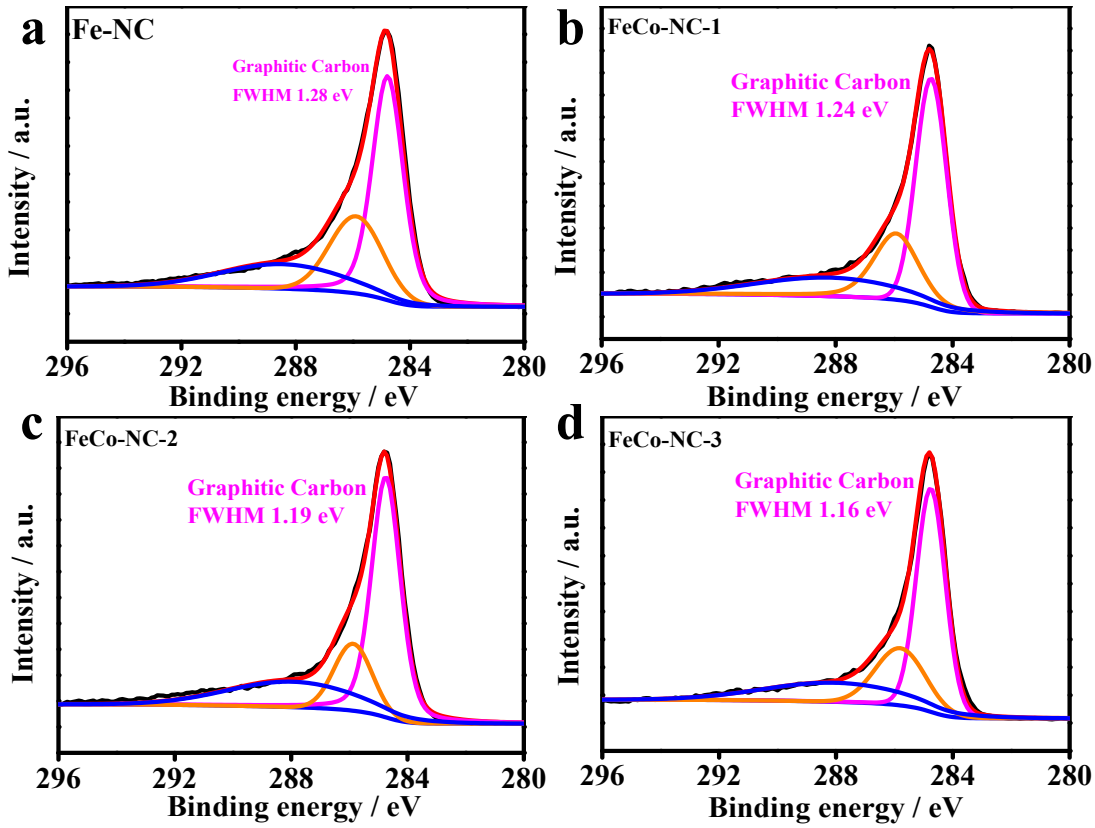

Figure. S11 The high-resolution C1s XPS spectra of various catalysts

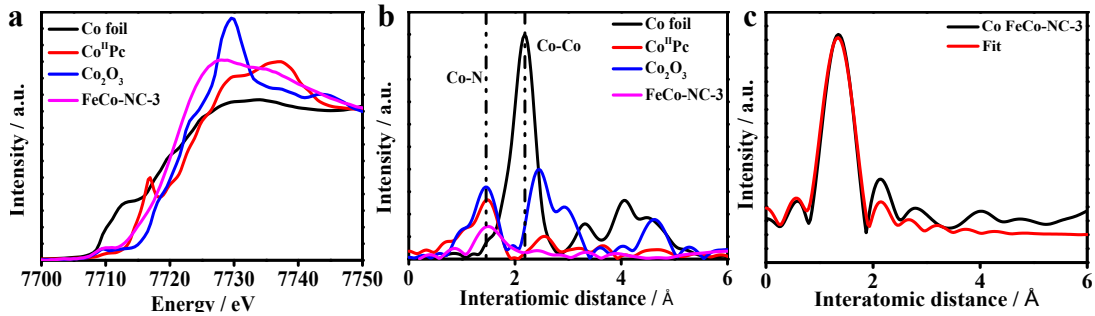

Figure. S12 (a) Co XANES spectra and (b) Co EXAFS spectra of Fe-NC, FeCo-NC-X, CoO, Co_2O_3, Co foil and CoPc; (c) corresponding Co K-edge EXAFS fitting.

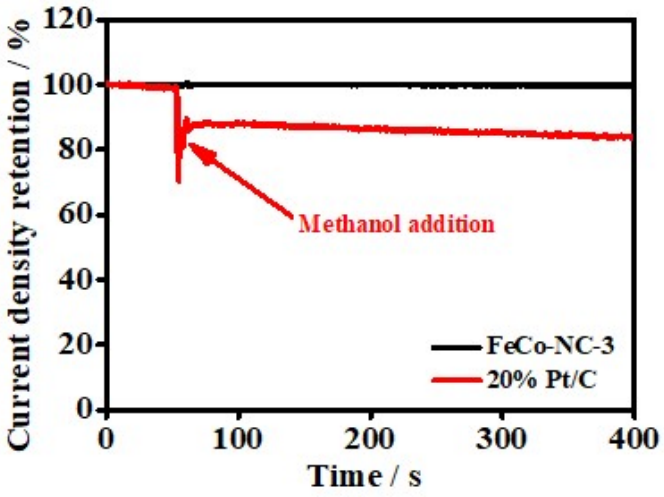

Figure. S13 Current density retention curves of FeCo-NC-3 and 20% Pt/C at 0.5 V in 0.1 M $HClO_4$ with addition of methanol.

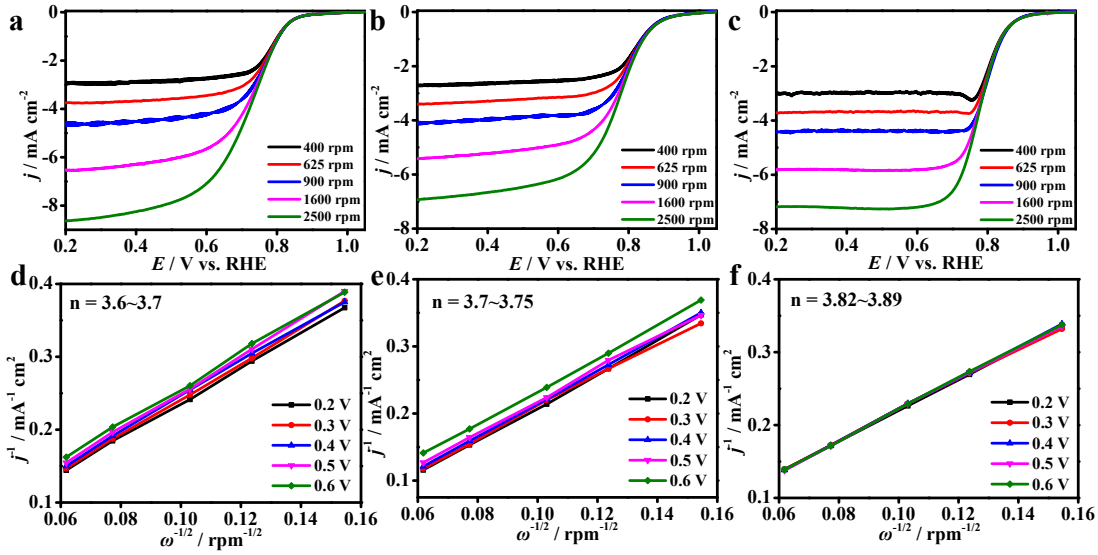

Figure. S14 LSV curves and K-L plots of (a, d) Fe-NC, (b, e) FeCo-NC-1 and (c, f) FeCo-NC-2 in O_2-saturated 0.1 M $HClO_4$ solution.

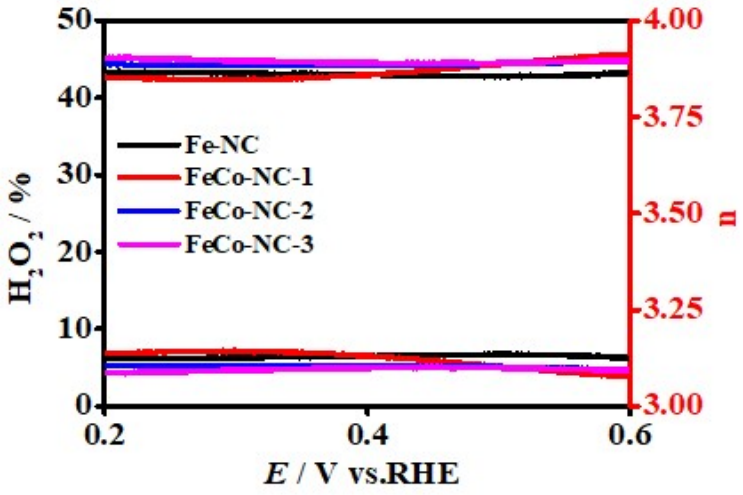

Figure. S15 H_2O_2 yield and electron transfer number for Fe-NC, FeCo-NC-1, FeCo-NC-2, and FeCo-NC-3 in 0.1 M $HClO_4$.

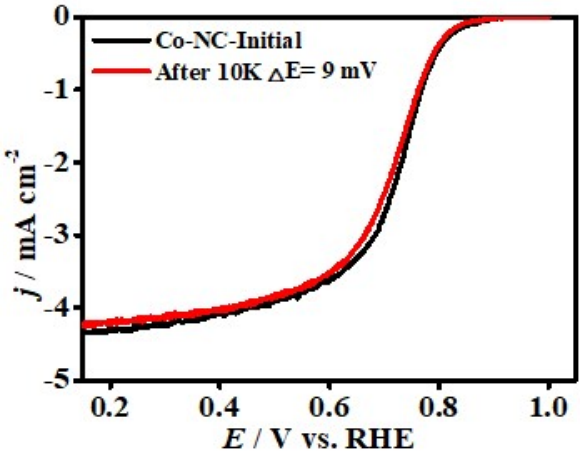

Figure. S16 ORR polarization curves before and after the stability test for Co-NC in 0.1 M $HClO_4$.

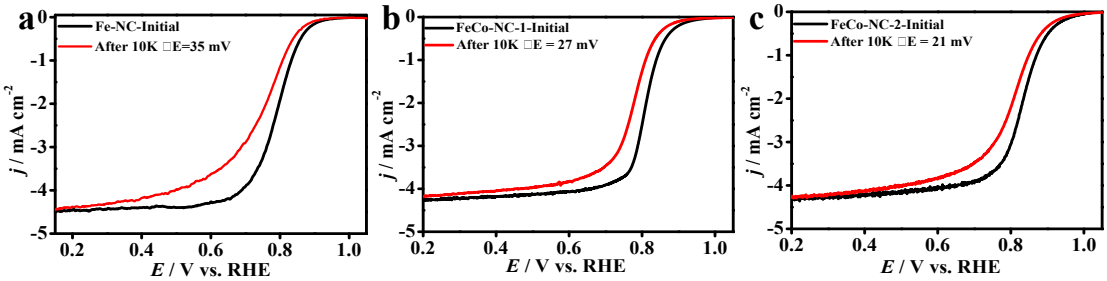

Figure. S17 ORR polarization curves before and after the stability test for (a) Fe-NC, (b) FeCo-NC-1 and (c) FeCo-NC-2 in 0.1 M $HClO_4$.

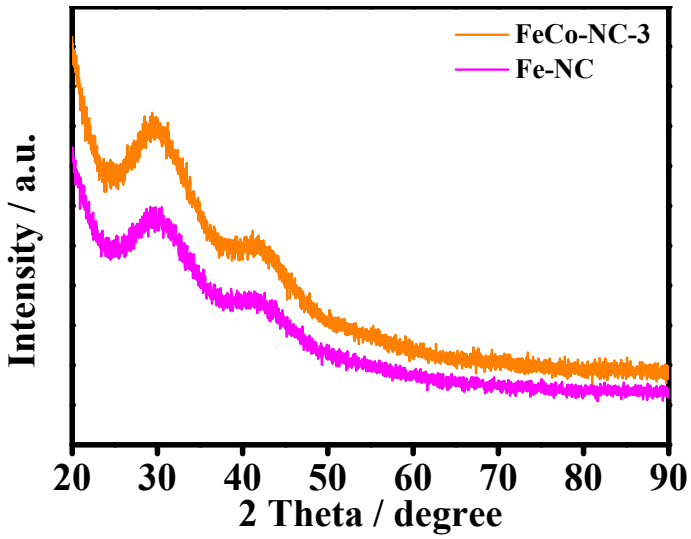

Figure. S18 The XRD patterns of Fe-NC and FeCo-NC-3 after 10000-cycle ADT.

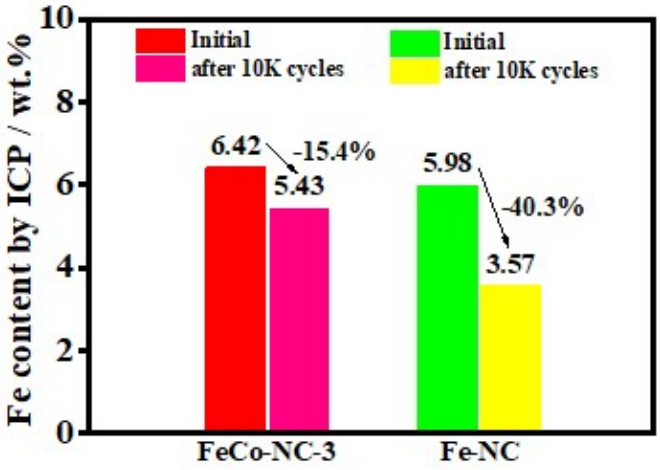

Figure. S19 Fe content by ICP measurements before and after 10k cycles.

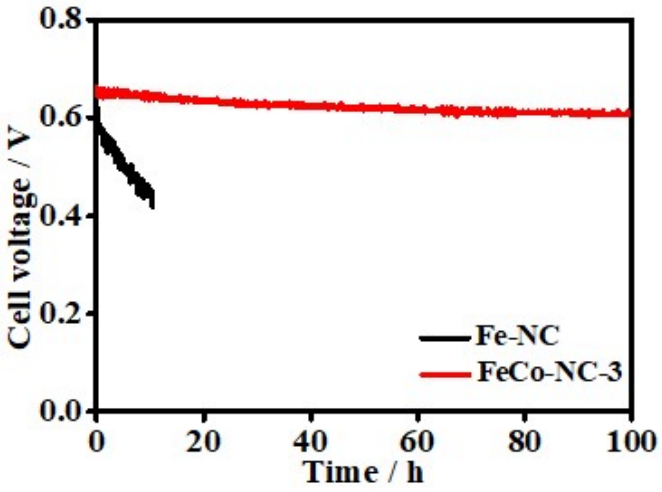

Figure. S20 Stability test at a constant current density of 0.4 A cm^{-2} of FeCo-NC-3 and Fe-NC in PEMFC. (Backpressure: 2 bar; Cell temperature: 80°C; H_2/O_2 flow rate: 400 mL min^{-1})

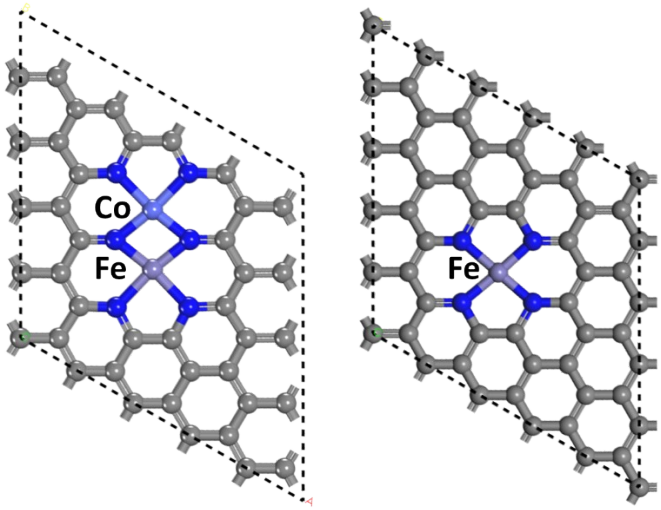

Figure. S21 Top view of the $FeCoN_6$(left) and Fe-N_4(right) slab.

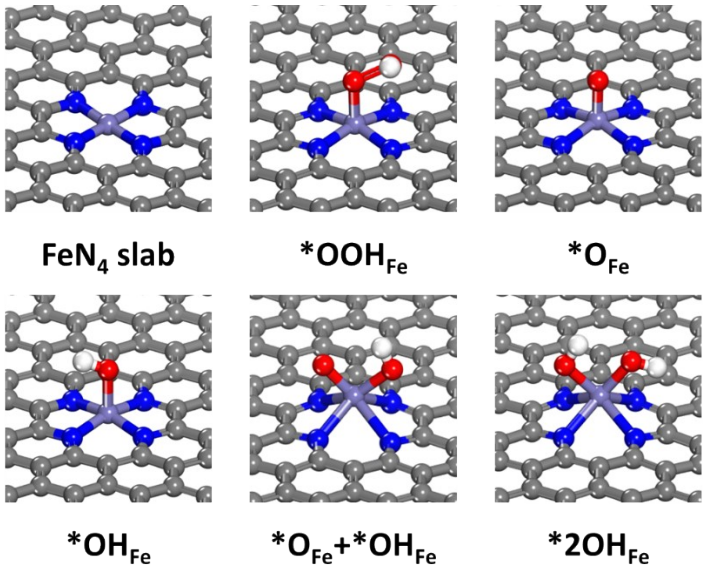

Figure. S22 Intermediate structures over Fe-N_4 slab.

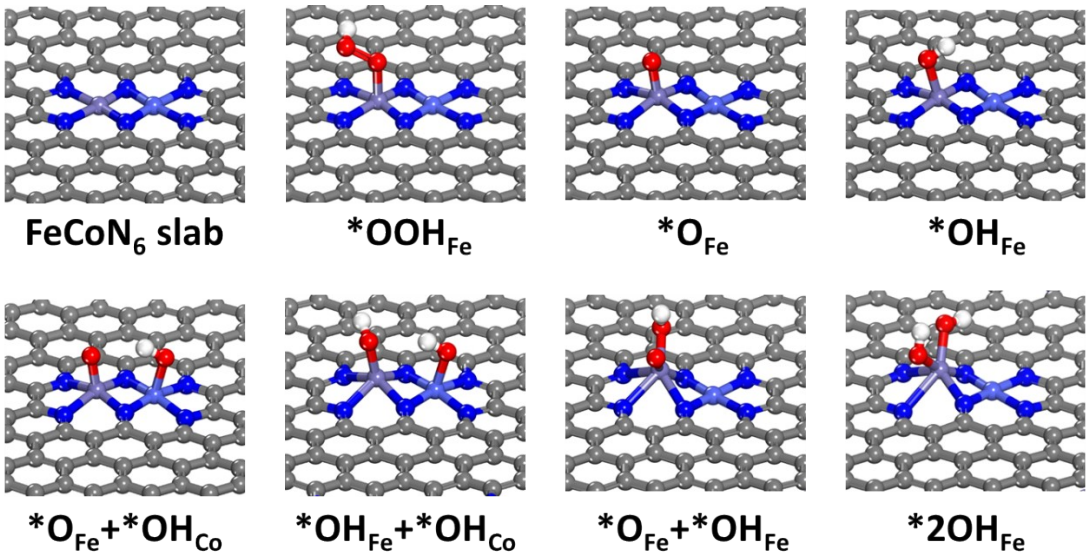

Figure. S23 Intermediate structures over $FeCoN_6$ slab.

Table S1 BET surface area and pore volume of several Fe-NC and FeCo-NC-X samples.

	BET surface area / $m^2\ g^{-1}$	Micropore area / $m^2\ g^{-1}$	Pore volume / $cm^3\ g^{-1}$
Fe-NC	585	464.6	0.68
FeCo-NC-1	558.9	452.1	0.66
FeCo-NC-2	536	442.4	0.58
FeCo-NC-3	536.7	466	0.64

Table S2 The elemental content of N, Fe and Co derived from the XPS survey and ICP-OES for all samples.

	N (at. %)[a]	Fe (at. %)[a]	Co (at. %)[a]	Fe (wt. %)[b]	Co (wt. %)[b]
Fe-NC	7.64	1.57	/	5.98	/
FeCo-NC-1	7.37	1.36	0.59	6.01	1.37
FeCo-NC-2	7.59	1.4	0.69	6.35	1.71
FeCo-NC-3	7.17	1.38	0.88	6.42	1.98

Table S3 Summary of the Mossbauer parameters and assignments to different Iron species in Fe-NC and FeCo-NC-3 catalysts.

	Fe species	IS / mm s^{-1}	QS / mm s^{-1}	Content / %
Fe-NC	D1	0.18	2.03	9.7
	D2	0.251	1.277	40.9
	D3	0.172	0.639	49.4
FeCo-NC-3	D1	0.13	2	12.1
	D2	0.248	1.21	25.9
	D3	0.119	0.639	62

Table S4 EXAFS fitting results of Fe-NC and FeCo-NC-3 catalysts.

	Path	C.N.	R (Å)	$\sigma^2\times10^3$ (Å^2)	ΔE (eV)	R factor
Fe-NC	Fe-N	5.4±1.8	1.98±0.01	11.9±2.4	-2.6±2.0	0.010
FeCo-NC-3	Fe-N	3.7±1.6	2.00±0.02	10.8±2.7	0.0±2.1	0.014
	Co-N	3.9±1.9	1.92±0.02	8.8±4.9	-4.2±4.0	0.015

Table S5 ORR activity and durability comparison of Fe-based catalysts in acidic media.

Catalysts	Electrolyte (mol L^{-1})	$E_{1/2}$ / V (vs . RHE)	Activity decay / mV	ref
FeCo-NC-3	0.1 $HClO_4$	0.842	11 @ 10000 cycles	This work
Fe-NC	0.1 $HClO_4$	0.803	35 @ 10000 cycles	This work
C-Fe-Z8-Ar	0.1 $HClO_4$	0.82	40 @ 10000 cycles	12
Fe-N/CNT-2	0.1 $HClO_4$	0.76	20 @ 500 cycles	13
0.17CVD/Fe-N-C-*kat*	0.5 H_2SO_4	0.835	20 @ 10000 cycles	14
Fe(Zn)-N-C	0.1 $HClO_4$	0.83	14 @ 10000 cycles	15
Fe,Mn/N-C	0.1 $HClO_4$	0.804	18 @ 8000 cycles	16
FeCoNx/C	0.1 $HClO_4$	0.86	13 @ 5000 cycles	17
FeCo-SAs-N-C	0.1 $HClO_4$	0.832	32 @ 10000 cycles	18
M/FeCo-SAs-N-C	0.1 $HClO_4$	0.851	17@ 10000 cycles	18
FeNi-N_6-C	0.1 $HClO_4$	0.80	12 @ 5000 cycles	19

Table S6 Comparisons of recently reported H2–O2 PEMFCs performance on SACs/ DACs.

Catalyst	T_{cell} [°C]	H_2/O_2 flow rate [mL min^{-1}]	Back pressure	Catalyst loading [mg cm^{-2}]	P_{max} [mW cm^{-2}]	Ref
FeCo-NC-3	80	1000/1000	2 bar	3.0	800	This work
HP-FeN_4	80	400/400	200 kpa	4.0	700	20
CPANI-Fe-NaCl	80	150/200	——	4.0	600	21
PFeTTPP-1000	80	300/300	1.5 bar	4.1	730	22
Fe2-Z8-C	80	300/400	2.5 bar	2.8	1141	23
Fe_2N_6	80	400/400	200 kpa	4.0	845	24
(Fe,Co)/N-C	80	——	0.2 Mpa	0.77	980	25
Fe/Ni-N_x/OC	80	200/200	1.0 bar	4.0	580	26
SA-Fe/NG	80	300/400	2.5 bar	4.0	870	27
Mn-N-C-HCl-800/1100	80	200/1000	1.0 bar	4.0	600	28
20 Mn-NC-second	80	200/200	1.0 bar	4.0	460	29

Reference

1. G. Kresse and J. Furthmuller, *Comput. Mater. Sci.*, 1996, **6**, 15-50.
2. G. Kresse and J. Furthmuller, *Phys. Rev. B* 1996, **54**, 11169-11186.
3. P. E. Blochl, *Phys. Rev. B*, 1994, **50**, 17953-17979.
4. G. Kresse and D. Joubert, *Phys. Rev. B* 1999, **59**, 1758-1775.
5. J. Wellendorff, K. T. Lundgaard, A. Mogelhoj, V. Petzold, D. D. Landis, J. K. Norskov, T. Bligaard and K. W. Jacobsen, *Phys. Rev. B*, 2012, **85**, 235149.
6. Z. W. Ulissi, A. J. Medford, T. Bligaard and J. K. Norskov, *Nat. Commun.*, 2017, **8**, 14621.
7. B. Wang, S. Chen, J. Zhang, S. Li and B. Yang, *J. Phys. Chem. C* 2019, **123**, 30389-30397.
8. T. Gu, B. Wang, S. Chen and B. Yang, *ACS Catal.*, 2020, **10**, 6346-6355.
9. R. Christensen, H. A. Hansen and T. Vegge, *Catal. Sci. Technol.*, 2015, **5**, 4946-4949.
10. J. K. Norskov, J. Rossmeisl, A. Logadottir, L. Lindqvist, J. R. Kitchin, T. Bligaard and H. Jonsson, *J. Phys. Chem. B*, 2004, **108**, 17886-17892.
11. V. J. Bukas, H. W. Kim, R. Sengpiel, K. Knudsen, J. Voss, B. D. McCloskey and A. C. Luntz, *ACS Catal.*, 2018, **8**, 11940-11951.
12. X. Wang, H. Zhang, H. Lin, S. Gupta, C. Wang, Z. Tao, H. Fu, T. Wang, J. Zheng, G. Wu and X. Li, *Nano Energy*, 2016, **25**, 110-119.
13. D. Xia, X. Yang, L. Xie, Y. Wei, W. Jiang, M. Dou, X. Li, J. Li, L. Gan and F. Kang, *Adv. Funct. Mater.*, 2019, **29**, 1906174.
14. S. Liu, M. Wang, X. Yang, Q. Shi, Z. Qiao, M. Lucero, Q. Ma, K. L. More, D. A. Cullen, Z. Feng and G. Wu, *Angew. Chem., Int. Ed.*, 2020, **59**, 21698-21705.
15. L. Gong, H. Zhang, Y. Wang, E. Luo, K. Li, L. Gao, Y. Wang, Z. Wu, Z. Jin, J. Ge, Z. Jiang, C. Liu and W. Xing, *Angew. Chem. Int. Ed.*, 2020, **59**, 13923-13928.
16. G. Yang, J. Zhu, P. Yuan, Y. Hu, G. Qu, B. A. Lu, X. Xue, H. Yin, W. Cheng, J. Cheng, W. Xu, J. Li, J. Hu, S. Mu and J. N. Zhang, *Nat. Commun.*, 2021, **12**,

1734.

17. M. Xiao, Y. Chen, J. Zhu, H. Zhang, X. Zhao, L. Gao, X. Wang, J. Zhao, J. Ge, Z. Jiang, S. Chen, C. Liu and W. Xing, *J. Am. Chem. Soc.*, 2019, **141**, 17763-17770.
18. S. H. Yin, J. Yang, Y. Han, G. Li, L. Y. Wan, Y. H. Chen, C. Chen, X. M. Qu, Y. X. Jiang and S. G. Sun, *Angew. Chem. Int. Ed.*, 2020, **59**, 21976-21979.
19. Y. Zhou, W. Yang, W. Utetiwabo, Y. M. Lian, X. Yin, L. Zhou, P. Yu, R. Chen and S. Sun, *J. Phys. Chem. Lett.*, 2020, **11**, 1404-1410.
20. N. Zhang, T. Zhou, M. Chen, H. Feng, R. Yuan, C. a. Zhong, W. Yan, Y. Tian, X. Wu, W. Chu, C. Wu and Y. Xie, *Energy Environ. Sci.*, 2020, **13**, 111-118.
21. W. Ding, L. Li, K. Xiong, Y. Wang, W. Li, Y. Nie, S. Chen, X. Qi and Z. Wei, *J. Am. Chem. Soc.*, 2015, **137**, 5414-5420.
22. S. Yuan, J.-L. Shui, L. Grabstanowicz, C. Chen, S. Commet, B. Reprogle, T. Xu, L. Yu and D.-J. Liu, *Angew. Chem., Int. Ed.*, 2013, **52**, 8349-8353.
23. Q. Liu, X. Liu, L. Zheng and J. Shui, *Angew. Chem. Int. Ed.*, 2018, **57**, 1204-1208.
24. N. Zhang, T. Zhou, J. Ge, Y. Lin, Z. Du, C. a. Zhong, W. Wang, Q. Jiao, R. Yuan, Y. Tian, W. Chu, C. Wu and Y. Xie, *Matter*, 2020, **3**, 509-521.
25. J. Wang, Z. Huang, W. Liu, C. Chang, H. Tang, Z. Li, W. Chen, C. Jia, T. Yao, S. Wei, Y. Wu and Y. Li, *J. Am. Chem. Soc.*, 2017, **139**, 17281-17284.
26. Z. Zhu, H. Yin, Y. Wang, C. H. Chuang, L. Xing, M. Dong, Y. R. Lu, G. Casillas-Garcia, Y. Zheng, S. Chen, Y. Dou, P. Liu, Q. Cheng and H. Zhao, *Adv. Mater.*, 2020, **32**, 2004670.
27. L. Yang, D. Cheng, H. Xu, X. Zeng, X. Wan, J. Shui, Z. Xiang and D. Cao, *Proc. Natl. Acad. Sci. U.S.A.*, 2018, **115**, 6626-6631.
28. M. Chen, X. Li, F. Yang, B. Li, T. Stracensky, S. Karakalos, S. Mukerjee, Q. Jia, D. Su, G. Wang, G. Wu and H. Xu, *ACS Catal.*, 2020, **10**, 10523-10534.
29. J. Li, M. Chen, D. A. Cullen, S. Hwang, M. Wang, B. Li, K. Liu, S. Karakalos, M. Lucero, H. Zhang, C. Lei, H. Xu, G. E. Sterbinsky, Z. Feng, D. Su, K. L. More, G. Wang, Z. Wang and G. Wu, *Nat. Catal.*, 2018, **1**, 935-945.